

World Journal of *Clinical Cases*

World J Clin Cases 2022 August 26; 10(24): 8432-8807



EDITORIAL

- 8432 Evolution of *World Journal of Clinical Cases* over the past 5 years
Muthu S

OPINION REVIEW

- 8436 NF- κ B: A novel therapeutic pathway for gastroesophageal reflux disease?
Zhang ML, Ran LQ, Wu MJ, Jia QC, Qin ZM, Peng YG

MINIREVIEWS

- 8443 Obligate aerobic, gram-positive, weak acid-fast, nonmotile bacilli, *Tsukamurella tyrosinosolvans*: Minireview of a rare opportunistic pathogen
Usuda D, Tanaka R, Suzuki M, Shimozawa S, Takano H, Hotchi Y, Tokunaga S, Osugi I, Katou R, Ito S, Mishima K, Kondo A, Mizuno K, Takami H, Komatsu T, Oba J, Nomura T, Sugita M
- 8450 Diffusion tensor imaging pipeline measures of cerebral white matter integrity: An overview of recent advances and prospects
Safri AA, Nassir CMNCM, Iman IN, Mohd Taib NH, Achuthan A, Mustapha M
- 8463 Graft choices for anterolateral ligament knee reconstruction surgery: Current concepts
Chalidis B, Pitsilos C, Kitridis D, Givissis P
- 8474 Overview of the anterolateral complex of the knee
Garcia-Mansilla I, Zicaro JP, Martinez EF, Astoul J, Yacuzzi C, Costa-Paz M
- 8482 Complication of lengthening and the role of post-operative care, physical and psychological rehabilitation among fibula hemimelia
Salimi M, Sarallah R, Javanshir S, Mirghaderi SP, Salimi A, Khanzadeh S

ORIGINAL ARTICLE**Clinical and Translational Research**

- 8490 Pyroptosis-related genes play a significant role in the prognosis of gastric cancer
Guan SH, Wang XY, Shang P, Du QC, Li MZ, Xing X, Yan B

Retrospective Study

- 8506 Effects of propofol combined with lidocaine on hemodynamics, serum adrenocorticotrophic hormone, interleukin-6, and cortisol in children
Shi S, Gan L, Jin CN, Liu RF
- 8514 Correlation analysis of national elite Chinese male table tennis players' shoulder proprioception and muscle strength
Shang XD, Zhang EM, Chen ZL, Zhang L, Qian JH

- 8525** Clinical value of contrast-enhanced ultrasound in early diagnosis of small hepatocellular carcinoma (≤ 2 cm)

Mei Q, Yu M, Chen Q

- 8535** Identification of predictive factors for post-transarterial chemoembolization liver failure in hepatocellular carcinoma patients: A retrospective study

Yuan M, Chen TY, Chen XR, Lu YF, Shi J, Zhang WS, Ye C, Tang BZ, Yang ZG

- 8547** Clinical significance of half-hepatic blood flow occlusion technology in patients with hepatocellular carcinoma with cirrhosis

Liu D, Fang JM, Chen XQ

- 8556** Which octogenarian patients are at higher risk after cholecystectomy for symptomatic gallstone disease? A single center cohort study

D'Acapito F, Solaini L, Di Pietrantonio D, Tauceri F, Mirarchi MT, Antelmi E, Flamini F, Amato A, Framarini M, Ercolani G

Clinical Trials Study

- 8568** Computed tomography combined with gastroscopy for assessment of pancreatic segmental portal hypertension

Wang YL, Zhang HW, Lin F

Observational Study

- 8578** Psychological needs of parents of children with complicated congenital heart disease after admitting to pediatric intensive care unit: A questionnaire study

Zhu JH, Jin CD, Tang XM

Prospective Study

- 8587** Quantitative differentiation of malignant and benign thyroid nodules with multi-parameter diffusion-weighted imaging

Zhu X, Wang J, Wang YC, Zhu ZF, Tang J, Wen XW, Fang Y, Han J

Randomized Controlled Trial

- 8599** Application of unified protocol as a transdiagnostic treatment for emotional disorders during COVID-19: An internet-delivered randomized controlled trial

Yan K, Yusufi MH, Nazari N

- 8615** High-flow nasal cannula oxygen therapy during anesthesia recovery for older orthopedic surgery patients: A prospective randomized controlled trial

Li XN, Zhou CC, Lin ZQ, Jia B, Li XY, Zhao GF, Ye F

SYSTEMATIC REVIEWS

- 8625** Assessment tools for differential diagnosis of neglect: Focusing on egocentric neglect and allocentric neglect

Lee SH, Lim BC, Jeong CY, Kim JH, Jang WH

CASE REPORT

- 8634** Exome analysis for Cronkhite-Canada syndrome: A case report
Li ZD, Rong L, He YJ, Ji YZ, Li X, Song FZ, Li XA
- 8641** Discrepancy between non-invasive prenatal testing result and fetal karyotype caused by rare confined placental mosaicism: A case report
Li Z, Lai GR
- 8648** Paroxysmal speech disorder as the initial symptom in a young adult with anti-N-methyl-D-aspartate receptor encephalitis: A case report
Hu CC, Pan XL, Zhang MX, Chen HF
- 8656** Anesthetics management of a renal angiomyolipoma using pulse pressure variation and non-invasive cardiac output monitoring: A case report
Jeon WJ, Shin WJ, Yoon YJ, Park CW, Shim JH, Cho SY
- 8662** Traumatic giant cell tumor of rib: A case report
Chen YS, Kao HW, Huang HY, Huang TW
- 8667** Analysis of two naval pilots' ejection injuries: Two case reports
Zeng J, Liu XP, Yi JC, Lu X, Liu DD, Jiang YQ, Liu YB, Tian JQ
- 8673** Beware of the DeBakey type I aortic dissection hidden by ischemic stroke: Two case reports
Chen SQ, Luo WL, Liu W, Wang LZ
- 8679** Unilateral lichen planus with Blaschko line distribution: A case report
Dong S, Zhu WJ, Xu M, Zhao XQ, Mou Y
- 8686** Clinical features and progress of ischemic gastritis with high fatalities: Seven case reports
Shionoya K, Sasaki A, Moriya H, Kimura K, Nishino T, Kubota J, Sumida C, Tasaki J, Ichita C, Makazu M, Masuda S, Koizumi K, Kawachi J, Tsukiyama T, Kako M
- 8695** Retinoblastoma in an older child with secondary glaucoma as the first clinical presenting symptom: A case report
Zhang Y, Tang L
- 8703** Recurrent herpes zoster in a rheumatoid arthritis patient treated with tofacitinib: A case report and review of the literature
Lin QX, Meng HJ, Pang YY, Qu Y
- 8709** Intra-abdominal ectopic bronchogenic cyst with a mucinous neoplasm harboring a *GNAS* mutation: A case report
Murakami T, Shimizu H, Yamazaki K, Nojima H, Usui A, Kosugi C, Shuto K, Obi S, Sato T, Yamazaki M, Koda K
- 8718** Effects of intravascular photobiomodulation on motor deficits and brain perfusion images in intractable myasthenia gravis: A case report
Lan CH, Wu YC, Chiang CC, Chang ST

- 8728** Spontaneous acute epidural hematoma secondary to skull and dural metastasis of hepatocellular carcinoma: A case report
Lv GZ, Li GC, Tang WT, Zhou D, Yang Y
- 8735** Malignant melanotic nerve sheath tumors in the spinal canal of psammomatous and non-psammomatous type: Two case reports
Yeom JA, Song YS, Lee IS, Han IH, Choi KU
- 8742** When should endovascular gastrointestinal anastomosis transection Glissonean pedicle not be used in hepatectomy? A case report
Zhao J, Dang YL
- 8749** VARS2 gene mutation leading to overall developmental delay in a child with epilepsy: A case report
Wu XH, Lin SZ, Zhou YQ, Wang WQ, Li JY, Chen QD
- 8755** Junctional bradycardia in a patient with COVID-19: A case report
Aedh AI
- 8761** Application of 3 dimension-printed injection-molded polyether ether ketone lunate prosthesis in the treatment of stage III Kienböck's disease: A case report
Yuan CS, Tang Y, Xie HQ, Liang TT, Li HT, Tang KL
- 8768** High scored thyroid storm after stomach cancer perforation: A case report
Baik SM, Pae Y, Lee JM
- 8775** Cholecystitis-an uncommon complication following thoracic duct embolization for chylothorax: A case report
Dung LV, Hien MM, Tra My TT, Luu DT, Linh LT, Duc NM
- 8782** Endometrial squamous cell carcinoma originating from the cervix: A case report
Shu XY, Dai Z, Zhang S, Yang HX, Bi H
- 8788** Type 2 autoimmune pancreatitis associated with severe ulcerative colitis: Three case reports
Ghali M, Bensted K, Williams DB, Ghaly S
- 8797** Diffuse uterine leiomyomatosis: A case report and review of literature
Ren HM, Wang QZ, Wang JN, Hong GJ, Zhou S, Zhu JY, Li SJ

LETTER TO THE EDITOR

- 8805** Comment on "Posterior reversible encephalopathy syndrome in a patient with metastatic breast cancer: A case report"
Kunić S, Ibrahimagić OĆ, Kojić B, Džananović D

ABOUT COVER

Editorial Board Member of *World Journal of Clinical Cases*, Ahmed Mohamed Ahmed Al-Emam, PhD, Associate Professor, Department of Pathology, King Khalid University, Abha 62521, Saudi Arabia. amalemam@kku.edu.sa

AIMS AND SCOPE

The primary aim of *World Journal of Clinical Cases* (*WJCC*, *World J Clin Cases*) is to provide scholars and readers from various fields of clinical medicine with a platform to publish high-quality clinical research articles and communicate their research findings online.

WJCC mainly publishes articles reporting research results and findings obtained in the field of clinical medicine and covering a wide range of topics, including case control studies, retrospective cohort studies, retrospective studies, clinical trials studies, observational studies, prospective studies, randomized controlled trials, randomized clinical trials, systematic reviews, meta-analysis, and case reports.

INDEXING/ABSTRACTING

The *WJCC* is now abstracted and indexed in Science Citation Index Expanded (SCIE, also known as SciSearch®), Journal Citation Reports/Science Edition, Current Contents®/Clinical Medicine, PubMed, PubMed Central, Scopus, Reference Citation Analysis, China National Knowledge Infrastructure, China Science and Technology Journal Database, and Superstar Journals Database. The 2022 Edition of Journal Citation Reports® cites the 2021 impact factor (IF) for *WJCC* as 1.534; IF without journal self cites: 1.491; 5-year IF: 1.599; Journal Citation Indicator: 0.28; Ranking: 135 among 172 journals in medicine, general and internal; and Quartile category: Q4. The *WJCC*'s CiteScore for 2021 is 1.2 and Scopus CiteScore rank 2021: General Medicine is 443/826.

RESPONSIBLE EDITORS FOR THIS ISSUE

Production Editor: *Ying-Yi Yuan*; Production Department Director: *Xu Guo*; Editorial Office Director: *Jin-Lei Wang*.

NAME OF JOURNAL

World Journal of Clinical Cases

ISSN

ISSN 2307-8960 (online)

LAUNCH DATE

April 16, 2013

FREQUENCY

Thrice Monthly

EDITORS-IN-CHIEF

Bao-Gan Peng, Jerzy Tadeusz Chudek, George Kontogeorgos, Maurizio Serati, Ja Hyeon Ku

EDITORIAL BOARD MEMBERS

<https://www.wjgnet.com/2307-8960/editorialboard.htm>

PUBLICATION DATE

August 26, 2022

COPYRIGHT

© 2022 Baishideng Publishing Group Inc

INSTRUCTIONS TO AUTHORS

<https://www.wjgnet.com/bpg/gerinfo/204>

GUIDELINES FOR ETHICS DOCUMENTS

<https://www.wjgnet.com/bpg/GerInfo/287>

GUIDELINES FOR NON-NATIVE SPEAKERS OF ENGLISH

<https://www.wjgnet.com/bpg/gerinfo/240>

PUBLICATION ETHICS

<https://www.wjgnet.com/bpg/GerInfo/288>

PUBLICATION MISCONDUCT

<https://www.wjgnet.com/bpg/gerinfo/208>

ARTICLE PROCESSING CHARGE

<https://www.wjgnet.com/bpg/gerinfo/242>

STEPS FOR SUBMITTING MANUSCRIPTS

<https://www.wjgnet.com/bpg/GerInfo/239>

ONLINE SUBMISSION

<https://www.f6publishing.com>

Prospective Study

Quantitative differentiation of malignant and benign thyroid nodules with multi-parameter diffusion-weighted imaging

Xiang Zhu, Jia Wang, Yan-Chun Wang, Ze-Feng Zhu, Jian Tang, Xiao-Wei Wen, Ying Fang, Jun Han

Specialty type: Radiology, nuclear medicine and medical imaging**Provenance and peer review:**

Unsolicited article; Externally peer reviewed.

Peer-review model: Single blind**Peer-review report's scientific quality classification**

Grade A (Excellent): 0

Grade B (Very good): B

Grade C (Good): 0

Grade D (Fair): D

Grade E (Poor): 0

P-Reviewer: Chisthi MM, India; Zahran M, Egypt**Received:** September 10, 2021**Peer-review started:** September 10, 2021**First decision:** January 18, 2022**Revised:** January 25, 2022**Accepted:** July 19, 2022**Article in press:** July 19, 2022**Published online:** August 26, 2022**Xiang Zhu, Jia Wang, Yan-Chun Wang, Ze-Feng Zhu, Jun Han**, Department of Radiology, The First Hospital of Jiaying & The Affiliated Hospital of Jiaying University, Jiaying 314000, Zhejiang Province, China**Jian Tang**, Department of Head and Neck Surgery, the First Hospital of Jiaying & The Affiliated Hospital of Jiaying University, Jiaying 314000, Zhejiang Province, China**Xiao-Wei Wen, Ying Fang**, Department of Pathology, The First Hospital of Jiaying & The Affiliated Hospital of Jiaying University, Jiaying 314000, Zhejiang Province, China**Corresponding author:** Jun Han, MD, Associate Chief Physician, Department of Radiology, The First Hospital of Jiaying & The Affiliated Hospital of Jiaying University, 1882 Zhonghuan South Road, Jiaying 314000, Zhejiang Province, China. 13706735435@163.com

Abstract

BACKGROUND

The value of conventional magnetic resonance imaging in the differential diagnosis of thyroid nodules is limited; however, the value of multi-parameter diffusion-weighted imaging (DWI) in the quantitative evaluation of thyroid nodules has not been well determined.

AIM

To determine the utility of multi-parametric DWI including mono-exponential, bi-exponential, stretched exponential, and kurtosis models for the differentiation of thyroid lesions.

METHODS

Seventy-nine patients (62 with benign and 17 with malignant nodules) underwent multi-b value diffusion-weighted imaging of the thyroid. Multiple DWI parameters were obtained for statistical analysis.

RESULTS

Good agreement was found for diffusion parameters of thyroid nodules. Malignant lesions displayed lower diffusion parameters including apparent diffusion coefficient (ADC), the true diffusion coefficient (D), the perfusion fraction (f), the distributed diffusion coefficient (DDC), the intravoxel water diffusion heterogeneity (α) and kurtosis model-derived ADC (Dapp), and higher apparent diffusional kurtosis (Kapp) than benign entities (all $P < 0.01$), except for

the pseudodiffusion coefficient (D^*) ($P > 0.05$). The area under the ROC curve (AUC) of the $ADC_{(0 \text{ and } 1000)}$ was not significantly different from that of the $ADC_{(0 \text{ and } 2000)}$, $ADC_{(0 \text{ to } 2000)}$, $ADC_{(0 \text{ to } 1000)}$, D , DDC , $Dapp$ and $Kapp$ (all $P > 0.05$), but was significantly higher than the AUC of D^* , f and α (all $P < 0.05$) for differentiating benign from malignant lesions.

CONCLUSION

Multiple DWI parameters including ADC , D , f , DDC , α , $Dapp$ and $Kapp$ could discriminate benign and malignant thyroid nodules. The metrics including D , DDC , $Dapp$ and $Kapp$ provide additional information with similar diagnostic performance of ADC , combination of these metrics may contribute to differentiate benign and malignant thyroid nodules. The ADC calculated with higher b values may not lead to improved diagnostic performance.

Key Words: Thyroid nodule; Magnetic resonance imaging; Diffusion-weighted imaging; Quantitative study; Sensitivity; Specificity

©The Author(s) 2022. Published by Baishideng Publishing Group Inc. All rights reserved.

Core Tip: Multiple diffusion coefficient parameters obtained by fitting with mono-exponential, bi-exponential, stretched exponential, and kurtosis diffusion-weighted imaging models are feasible techniques for investigating thyroid nodules; The metrics including D , distributed diffusion coefficient, $Dapp$ and $Kapp$ provide additional information with similar diagnostic performance of ADC , and combination of these metrics may contribute to differentiate benign and malignant thyroid nodules; The apparent diffusion coefficient calculated with a mono-exponential model using a single pair of conventional b values ($b = 1000 \text{ s/mm}^2$) have similar diagnostic performance to those calculated with higher b values ($b \text{ value} > 1000 \text{ s/mm}^2$).

Citation: Zhu X, Wang J, Wang YC, Zhu ZF, Tang J, Wen XW, Fang Y, Han J. Quantitative differentiation of malignant and benign thyroid nodules with multi-parameter diffusion-weighted imaging. *World J Clin Cases* 2022; 10(24): 8587-8598

URL: <https://www.wjgnet.com/2307-8960/full/v10/i24/8587.htm>

DOI: <https://dx.doi.org/10.12998/wjcc.v10.i24.8587>

INTRODUCTION

Thyroid nodules are common lesions that occur thyroid cells growth into an abnormal lump within the thyroid gland; these nodules are often palpable and radiologically distinct from the surrounding parenchyma[1,2]. As with most common endocrine tumors, thyroid nodules have a reported prevalence of 4%-7% in the adult population on physical examination (identified by palpation), and 10 times more nodules are identified with imaging studies[1]. Approximately 5% of detected thyroid nodules are diagnosed as malignancies[3]. The incidence of thyroid cancer has continuously and sharply increased worldwide at a rate higher than any other cancer and has tripled over the past three decades[4-6].

The treatment options recommended for benign and malignant thyroid lesions are completely different; surgical treatment is recommended for the vast majority of thyroid cancer, while most benign nodules can be safely followed with an active surveillance management approach[2]. Therefore, initial management recommendations are very dependent on preoperative studies designed to distinguish between malignant and benign thyroid nodules[1,2,7]. Ultrasonography (US) has been used as the first-line imaging modality for patients with known or suspected thyroid cancer[8]. US also provides guidance for fine-needle aspiration biopsy (FNAB). However, evaluation by US is operator-dependent, and no single sonographic feature is of sufficient diagnostic value to accurately differentiate malignant nodules from benign nodules[9]. Although FNAB is the most accurate tool for evaluating thyroid nodules, it is an invasive procedure associated with possible complications, and its accuracy may vary depending on many factors, such as the skills of the operator and the location of aspiration[7,9].

Currently, diffusion-weighted imaging (DWI) is becoming a very useful tool for the detection and characterization of head and neck cancer. Restricted and hindered diffusion of water molecules within malignant tumors lead to high contrast on diffusion-weighted (DW) images compared with images of normal tissues thus facilitating the diagnosis. The acquired DW images are often postprocessed using standard mono-exponential fitting, which applies a linear shape to obtain apparent diffusion coefficient (ADC) maps. More restricted diffusion is observed in malignant tumors than in benign lesions, which is indicated by a reduction in the ADC[10]. Previous studies of thyroid cancer have indicated that ADC

parameters can distinguish malignant and benign thyroid nodules. In routine practice, however, the b values applied in thyroid DWI studies are usually lower than 1000 s/mm^2 . Moreover, the diagnostic performance of the ADC calculated with higher b values (b value $> 1000 \text{ s/mm}^2$) has not been well investigated in patients with thyroid cancer.

The microscopic motion of water molecules detected by DWI is influenced by diffusion of water molecules and by microcirculation of blood in capillary networks[10]. A specialized bi-exponential model known as intravoxel incoherent motion (IVIM) can separate the incoherent motion of water molecules in the randomly oriented capillaries from molecular diffusion in the extravascular space[10, 11]. In addition, these two components can be quantitatively expressed by three parameters: The true diffusion coefficient (D), the pseudodiffusion coefficient (D^*), and the perfusion fraction (f)[10,11]. Recently, only one study used IVIM to evaluate thyroid cancer and reported that IVIM data might be helpful for differentiating malignant thyroid nodules from benign nodules[10].

Different from the bi-exponential model, the stretched exponential DWI model has been recently proposed by Bennett *et al*[12] and provides a measure of signal deviation from the mono-exponential behavior caused by pseudoperfusion effects; thus, this model provides information on tissue heterogeneity and diffusion simultaneously with two parameters: the distributed diffusion coefficient (DDC) and the intravoxel water diffusion heterogeneity (α)[11,13,14]. In addition, diffusion kurtosis models yield an estimate of the excess kurtosis of the diffusion displacement probability distribution with two parameters, D_{app} and K_{app} , which are produced from the DKI model and represent the diffusion coefficient and the diffusional kurtosis, respectively. To the best of our knowledge, this is the first study to evaluate thyroid nodules with ADCs calculated with higher b values (b value $> 1000 \text{ s/mm}^2$) and to compare the diagnostic performance of diffusion parameters fitted by mono-exponential, bi-exponential, stretched exponential, and kurtosis DWI models to quantitatively differentiate thyroid cancer.

The aim of this study was to prospectively evaluate the following: (1) To determine whether ADCs calculated with higher b values (b value $> 1000 \text{ s/mm}^2$) had benefits over ADCs calculated with conventional b values ($b = 1000 \text{ s/mm}^2$) to quantitatively differentiate thyroid cancer; and (2) to evaluate the feasibility and diagnostic performance of using multiple diffusion coefficient parameters by fitting with mono-exponential (ADCs fitted with conventional and higher b values), bi-exponential (D , D^* and f), stretched exponential (DDC and α), and kurtosis DWI (D_{app} and K_{app}) models to quantitatively differentiate thyroid cancer.

MATERIALS AND METHODS

Patients

This study was approved by the First Hospital of Jiaxing Research and Ethics Committee. Written informed consent was obtained from all participants, and the hard copy was archived in the Department of Radiology at the First Hospital of Jiaxing. From January 2017 to July 2019, 79 consecutive patients with thyroid nodules determined by US who were scheduled to undergo thyroidectomy were prospectively enrolled. Multiparameter magnetic resonance imaging (MRI) examinations (including multiple b value DWI) were performed for each patient. The mean age of the included patients was 53 years (range, 20-72 years). Fifty-four of the 78 patients were female. All the patients enrolled in this study had been scheduled to undergo thyroidectomy within 2 wk. Histopathology revealed that 62 patients had benign nodules, including nodular goiter ($n = 48$) and thyroid adenoma ($n = 14$), while 17 patients had malignant nodules, including papillary thyroid carcinoma ($n = 12$), medullary thyroid carcinoma ($n = 4$), and follicular thyroid carcinoma ($n = 1$).

Image acquisition

All MRI examinations were performed in the prone position using a 3.0 Tesla (T) MRI scanner (Discovery MR750; GE Healthcare, United States) with an eight-channel neurovascular phased-array coil. Patients were instructed to breathe calmly and avoid swallowing as much as possible and practice this. The MRI examination consisted of conventional multiplanar (sagittal, axial, and coronal planar) T1- and T2-weighted imaging scans followed by multiple b value DWI scans. The duration of the whole examination was approximately 30 min. Multiple b value DWI was performed by using a standard, bipolar, single-shot echo-planar sequences in the axial plane. The DWI images were obtained with a repetition time/echo time (TR/TE) of 3000 ms/79.3 ms, section thickness of 4 mm, gap of 1.5 mm, field of view of $200 \text{ mm} \times 200 \text{ mm}$, and matrix of $128 \text{ mm} \times 128 \text{ mm}$. Parallel imaging was used with an acceleration factor of 2. A local shim box covering the thyroid was applied to minimize susceptibility artifacts. Thirteen b values from 0 to 2000 s/mm^2 (0, 30, 50, 80, 100, 150, 200, 400, 600, 800, 1000, 1500, and 2000 s/mm^2) were used in three orthogonal diffusion directions. The acquisition time for multiple b value DWI sequences was 1 min 57 s.

DWI images were transferred to a PC and postprocessed with mono-exponential, bi-exponential, stretched exponential, and kurtosis models using in-house software written in Matlab (version R2014b; MathWorks, Natick, MA, United States). Parameter maps were generated and included the mean ADC,

D, D^* , f , DDC, α , kurtosis model-derived ADC (D_{app}), and apparent diffusional kurtosis (K_{app}) values. Two independent thyroid radiologists (J.W. and X.Z. with 15 and 18 years of head and neck MR diagnostic experience, respectively) who were blinded to the histopathological results performed the postprocessing. The regions of interest were as large as possible to encompass the whole solid portion of the thyroid nodule while carefully avoiding areas of obvious necrosis, cystic degeneration, hemorrhagic, or calcified portions, according to T1-, T2-, and contrast-enhanced T1-weighted images for reference. The corresponding mathematical expressions are as follows.

Mono-exponential: ADC was automatically calculated by using the mono-exponential model with b values: $S(b) = S_0 \cdot \exp(-b \cdot ADC)$ where $S(b)$ is the diffusion sensitizing factor; S_0 is the signal intensity without a diffusion gradient; and $S(b)$ is the signal intensity at a particular b value. In our study, $ADC_{(0 \text{ and } 1000)}$ was calculated with b values of 0 s/mm² and 1000 s/mm², $ADC_{(0 \text{ to } 1000)}$ was calculated with b values from 0 s/mm² to 1000 s/mm² (0, 30, 50, 80, 100, 150, 200, 400, 600, 800, and 1000 s/mm²), $ADC_{(0 \text{ and } 2000)}$ was calculated with b values of 0 s/mm² and 2000 s/mm², $ADC_{(0 \text{ to } 2000)}$ was calculated with b values from 0 s/mm² to 2000 s/mm² (0, 30, 50, 80, 100, 150, 200, 400, 600, 800, 1000, 1500, and 2000 s/mm²).

Bi-exponential: According to the bi-exponential model, the mathematical relationship between b values and signal intensities was described using the following formula: $S(b) = S_0 \cdot [(1-f) \cdot \exp(-b \cdot D) + f \cdot \exp(-b \cdot D^*)]$ where $S(b)$ is the signal intensity at a particular b value; D is the true diffusion coefficient that reflects random motion of intra- and intercellular water molecules (slow component of diffusion); D^* is the diffusion parameter representing incoherent microcirculation within the voxel (perfusion related diffusion, or fast component of diffusion); and f is the fraction of the diffusion ($0 \leq f \leq 1$) linked to microcirculation.

Stretched exponential: By fitting the stretched exponential model, DDC and α were calculated as follows: $S(b) = S_0 \cdot \exp[-(b \cdot DDC)^\alpha]$ where DDC represents the distributed diffusion coefficient, and α represents the anomalous exponent term that parameterizes "tissue heterogeneity" ($0 \leq \alpha \leq 1$).

Kurtosis-exponential: The multi- b value DWI images fitted the following diffusion kurtosis imaging (DKI) signal decay equation:

$$S(b) = S_0 \cdot \exp(-b \cdot D_{app} + 1/6 \cdot b^2 D_{app}^2 K_{app})$$

where $S(b)$ is the signal intensity at a particular b value; D_{app} is the kurtosis model-derived ADC (in mm²/s); and K_{app} is the apparent diffusional kurtosis (dimensionless parameter), which suggest that the status of water molecular motion deviates from a Gaussian distribution. A minimum K_{app} value showed that the curve fit closely to a Gaussian distribution. However, increased K_{app} indicated increased contributions of the lesion area attributable to kurtosis behavior.

Histopathological examination

Histopathological examination findings from surgical specimens obtained after radical thyroidectomy or lobectomy were obtained from pathology reports, which were reviewed by two pathologists (X.W.W. and Y.F. with 25 and 18 years of experience with pathological diagnosis, respectively) specializes in the pathological diagnosis of thyroid diseases. According to the characteristics of the thyroid nodules, patients were divided into two groups. The benign tumor group included those with nodular goiter and thyroid adenoma. The malignant tumor group included those with papillary thyroid carcinoma, medullary thyroid carcinoma, and follicular thyroid carcinoma. Histological subtype was determined for all lesions by immunohistochemical analysis.

Statistical analysis

Data are presented as the mean \pm standard deviation (SD). All statistical analyses were performed using SPSS 17.0 (SPSS, Chicago, IL, United States). The Mann-Whitney U test was used to compare the diffusion parametric differences in the subgroups. A P value < 0.05 was deemed statistically significant. Interreader reliability between the two radiologists was assessed by using the intraclass correlation coefficient (ICC). According to Fleiss[15], an ICC of 0.4 represents poor agreement, a value of 0.75 represents good agreement, and a value between 0.4 and 0.75 represents fair to moderate agreement. Moreover, receiver operating characteristic (ROC) curves were generated to evaluate the diagnostic performance of diffusion parameters for detecting malignant tumors. Sensitivity and specificity were computed at the optimal cutoff value for each diffusion parameter that maximized the Youden index. The area under the ROC curve (AUC) was compared between the ADC and other diffusion parameters by using Z test.

RESULTS

T2-weighted images, ADC maps, D map, D^* map, f map, DDC map, α map, D_{app} map, K_{app} map, and histopathological maps of representative cases of the benign and malignant patient groups are shown in

Table 1 Interreader reproducibility of measurement of diffusion parameters of thyroid nodules

Diffusion parameter	ICC	95%CI
Mono-exponential		
ADC _(0 and 1000)	0.944	(0.852, 0.979)
ADC _(0 to 1000)	0.938	(0.898, 0.962)
ADC _(0 and 2000)	0.904	(0.844, 0.941)
ADC _(0 to 2000)	0.942	(0.905, 0.962)
Biexponential		
D	0.949	(0.921, 0.967)
D*	0.935	(0.900, 0.958)
f	0.897	(0.844, 0.933)
stretched exponential		
DDC	0.994	(0.990, 0.996)
α	0.973	(0.958, 0.983)
Kurtosis DWI		
Dapp	0.787	(0.685, 0.859)
Kapp	0.855	(0.782, 0.905)

ADC: Apparent diffusion coefficient; DWI: Diffusion-weighted imaging; D: Slow diffusion coefficient; D*: Fast diffusion coefficient; f: Fraction of fast diffusion; DDC: Distributed diffusion coefficient; ICC: Intraclass correlation; α : Anomalous exponent term; Dapp: Mean diffusivity; Kapp: Mean kurtosis.

Figures 1 and 2. In addition, the plot of the decay in diffusion-weighted signal intensity fitted by mono-exponential, bi-exponential, stretched-exponential, and kurtosis models, and fitted by a mono-exponential model with different b values for the benign and malignant thyroid nodules are shown in Figures 1 and 2.

The interobserver reproducibility between the two radiologists for determining thyroid nodule diffusion parameter measurements was calculated by using the ICC (Table 1). Good agreement was found for all metrics including ADC, D, D*, f, DDC, α , Dapp, and Kapp, indicating good reproducibility between the two readers. Therefore, the diffusion parameters measured by the first radiologist (Z.X.) were included for comparison. Table 2 shows the quantitative comparison of diffusion parameters between benign and malignant thyroid nodules. The diffusion parameters including ADC, D, f, DDC, α , and Dapp were significantly lower in malignant thyroid nodules than in benign nodules (all $P < 0.01$). Kapp was significantly higher in malignant thyroid nodules than in benign nodules ($P < 0.01$). D* was not significantly different between the two groups ($P > 0.05$).

The results of the ROC analyses of diffusion parameters for differentiating malignant nodules from benign nodules are summarized in Table 3. ROC curves of the ADC_(0 and 1000), ADC_(0 and 2000), ADC_(0 to 1000), ADC_(0 to 2000), D, D*, f, DDC, α , Dapp and Kapp are presented in Figure 3. ROC analysis demonstrated that ADC_(0 to 1000) metrics showed trends toward higher AUC values than the ADC_(0 and 1000), ADC_(0 and 2000), and ADC_(0 to 2000), using an ADC_(0 to 1000) cutoff value of 1.5×10^{-3} mm²/s, and malignant nodules could be diagnosed with a sensitivity of 72.6% and a specificity of 100%, but none of these differences reached statistical significance (all $P > 0.05$). The ADC_(0 and 1000), ADC_(0 to 1000), Kapp metrics had significantly higher AUC values than D*, f, and α (all $P < 0.05$). The ADC_(0 and 2000), ADC_(0 to 2000), and D metrics had significantly higher AUC values than D*, and f (all $P < 0.05$). The DDC, and Dapp metrics had significantly higher AUC values than D* (all $P < 0.05$).

DISCUSSION

To our best of knowledge, this work is the first study to investigate the feasibility of using multiple diffusion coefficient parameters by fitting with mono-exponential, bi-exponential, stretched exponential, and kurtosis DWI models to quantitatively differentiate malignant thyroid nodules from benign thyroid nodules. All parameters of the four models showed high interobserver agreement, suggesting that measurement of these parameters had good reproducibility and reliability.

Table 2 Comparison of diffusion parameters between benign and malignant thyroid nodules

Diffusion parameter	Benign nodules	Malignant nodules	P value
Mono-exponential			
ADC _(0 and 1000)	1.85 ± 0.24	1.29 ± 0.27	< 0.01
ADC _(0 to 1000)	1.79 ± 0.021	1.19 ± 0.23	< 0.01
ADC _(0 and 2000)	1.35 ± 0.15	0.95 ± 0.15	< 0.01
ADC _(0 to 2000)	1.41 ± 0.15	0.95 ± 0.15	< 0.01
Biexponential			
D	1.34 ± 0.41	0.89 ± 0.26	< 0.01
D*	22.08 ± 18.53	26.09 ± 20.87	> 0.05
f	0.38 ± 0.19	0.30 ± 0.14	< 0.01
Stretched exponential			
DDC	2.15 ± 0.62	1.45 ± 0.51	< 0.01
α	0.78 ± 0.19	0.67 ± 0.19	< 0.01
Kurtosis DWI			
Dapp	2.88 ± 0.73	2.11 ± 0.67	< 0.01
Kapp	0.57 ± 0.12	0.85 ± 0.19	< 0.01

ADC: Apparent diffusion coefficient; D: Slow diffusion coefficient; D*: Fast diffusion coefficient; f: Fraction of fast diffusion; DDC: Distributed diffusion coefficient; α : Anomalous exponent term; DWI: Diffusion-weighted imaging; Dapp: Mean diffusivity; Kapp, mean kurtosis. The ADC, D, D*, DDC, and Dapp are given in units of $\times 10^{-3}$ mm²/s. P values from statistical comparison between benign and malignant nodules were obtained by using the Mann-Whitney U test.

Previous studies on DWI in thyroid cancer have mostly focused on mono-exponential models with conventional b values (b value ≤ 1000 s/mm²), and most studies have suggested that ADCs of malignant lesions were significantly lower than those of benign lesions[9,16-19]. Similarly, in our study, the ADC_(0 and 1000) and ADC_(0 to 1000) showed that malignant thyroid lesions had significantly lower ADCs than benign lesions, with AUC values of 0.879 and 0.882, respectively. Generally, although higher b values might produce more susceptibility to distortions and could increase the noise in DWI images, higher b values produced more diffusion weighting and therefore higher contrast between lesions and normal tissue[16]. Recent reports have shown advantages of using a higher b value (b value > 1000 s/mm²) for DWI and ADC calculations for the diagnosis of acute stroke[20], malignant lymphoma[21], and prostate cancer[22]. In our study, although the ADC_(0 and 2000) and ADC_(0 to 2000) showed relatively higher sensitivities of 79.0% and 77.4%, respectively, than ADC_(0 and 1000) and ADC_(0 to 1000) sensitivities of 64.5% and 72.6%, respectively, the ADC_(0 and 2000) and ADC_(0 to 2000) showed similar diagnostic performance to the ADC_(0 and 1000) and ADC_(0 to 1000), with AUC values of 0.874 and 0.878, respectively. Thus, our study indicates that DWI acquired with regular b values (b = 1000 s/mm²) can be used to calculate DWI parameters similar to those obtained with DWI acquired with higher b values in patients with thyroid nodules. This phenomenon has also been reported by Eghtedari, M. on quantitative breast DWI for breast cancer[23]. Additionally, the ADC derived from a mono-exponential model with more than two b values is theoretically good for ADC fitting. In our study, the ADC_(0 to 1000) showed a relatively higher sensitivity of 72.6% than the that of the ADC_(0 and 1000) of 64.5%; the ADC_(0 to 2000) showed similar sensitivity of 77.4% to that of the ADC_(0 and 2000) of 79.0%. In addition, the diagnostic performance was similar between the ADC_(0 and 1000) and ADC_(0 to 1000) and between the ADC_(0 and 2000) and ADC_(0 to 2000). Therefore, if the ADC fitted with the mono-exponential model alone was used to differentiate malignant thyroid nodules from benign thyroid nodules, using a single pair of b values (usually 0 s/mm² and 1000 s/mm²) was acceptable for ADC calculation.

Bi-exponential IVIM DWI is a method initially proposed by Le Bihan *et al*[24] to quantitatively assess the microscopic motion that occurs at the subvoxel scale on MRI. D values mainly reflect the molecular diffusion of water protons. The D* value and f value mainly reflect perfusion status. In our study, the D values of malignant thyroid nodules were significantly lower than those of benign thyroid nodules. This finding was similar to the results of previous studies of thyroid cancer[10], breast cancer[11], nasopharyngeal carcinoma[25], prostate cancer[26], and metastatic lymph nodes in the head and neck[27]. This phenomenon might be due to the rapid cellular proliferation, high cell density and reduced extracellular space in malignant thyroid lesions. In addition, the AUC of the D was slightly lower than that of the ADC value obtained from the mono-exponential model but was not significantly different.

Table 3 Diagnostic performance of diffusion parameters for differentiating malignant thyroid nodules from benign thyroid nodules

Diffusion parameter	AUC	Cut-off value	Sensitivity, %	Specificity, %	Youden index	P value
Mono-exponential						
ADC _(0 and 1000)	0.879	1.6	64.5	100.0	0.645	Ref.
ADC _(0 and 2000)	0.874	1.1	79.0	88.2	0.672	0.94
ADC _(0 to 1000)	0.882	1.5	72.6	100.0	0.726	0.94
ADC _(0 to 2000)	0.878	1.1	77.4	88.2	0.656	0.99
Biexponential						
D	0.861	1.1	71.0	94.1	0.651	0.76
D*	0.643	22.2	88.2	56.5	0.447	< 0.01
f	0.709	0.37	46.8	100.0	0.468	< 0.05
Stretched exponential						
DDC	0.841	2.0	59.7	100.0	0.597	0.53
α	0.748	0.73	62.9	88.2	0.511	< 0.05
Kurtosis DWI						
Dapp	0.815	2.6	61.3	88.2	0.495	0.33
Kapp	0.889	0.65	100.0	74.2	0.742	0.84

AUC: Area under the receiver operating characteristic curve; ADC: Apparent diffusion coefficient; DWI: Diffusion-weighted imaging; D: Slow diffusion coefficient; D*: Fast diffusion coefficient; f: Fraction of fast diffusion; DDC: Distributed diffusion coefficient; α : Anomalous exponent term; Dapp: Mean diffusivity; Kapp: Mean kurtosis. The cut-off values for the ADC, D, D*, DDC, and Dapp are given in units of $\times 10^{-3}$ mm²/s. P values from statistical comparisons between the AUC values of the ADC_(0 and 1000) (Ref) and other diffusion parameters were obtained by using the method of Z test.

Regarding the perfusion-related metrics evaluated in our study, the f values of the malignant thyroid nodules were also significantly lower than those of benign thyroid nodules. However, Tan *et al*[10] reported that the f values of malignant thyroid tumors were significantly higher than those of benign lesions. In 2007, Tezelman *et al*[28] used dynamic contrast-enhanced (DCE) MRI to show that thyroid cancer had increased perfusion and blood volume compared with benign lesions. If perfusion is related to blood volume, the findings of their report are inconsistent with our evidence, which shows that the f value is significantly lower in thyroid cancer than in benign lesion. Our results with inconsistent perfusion values are also reflected by the results of other similar studies that have reported paradoxically lower f values in cancerous tissues[12,25-27]. A possible reason for this discrepancy may be explained by the theory that f values are not specific to perfusion alone but also be sensitive to other density phenomena[29]. Another possible reason is that f value is dependent on echo time (TE), at longer TE, the signal decays more at low b values, which would increase the estimated f values[30]. Hence, the lower f value in benign tumors may be related to parameters such as TE[30]. In the current study, the AUC of the f value was significantly lower than that of the ADC value obtained from the mono-exponential model. Although the mean D* value was slightly higher in malignant thyroid nodules than in benign thyroid nodules, the difference was not significant in our study. This finding is probably due to its sensitivity to noise, and the D* value has been shown to have poorer reproducibility than the f value in prior studies of the liver[14].

The stretched exponential diffusion model is an alternate method that can simultaneously assess both tissue heterogeneity and diffusion. Prior studies have reported that the stretched exponential diffusion model has better diagnostic performance for differentiating malignant from benign lesions than ADC parameters derived from a mono-exponential model in breast cancer and prostate cancer[31,32]. The DDC can be considered a weighted sum over a distribution of ADCs that represent multiexponential decay properties[31]. In our study, the DDC of the malignant thyroid nodule was significantly lower than that of benign thyroid nodules, but the results of the ROC curve analysis indicate that the diagnostic value of the DDC did not achieve a significant difference compared with ADC. The diffusion parameter α is supposed to represent intravoxel water diffusion heterogeneity. Values of α near 0 indicate high intravoxel diffusion heterogeneity. In our study, α was significantly lower in malignant thyroid nodules than in benign thyroid nodules, suggesting that malignant thyroid nodules exhibited higher intravoxel diffusion heterogeneity than the benign thyroid nodules. However, the diagnostic performance of α was lower than that of the ADC.

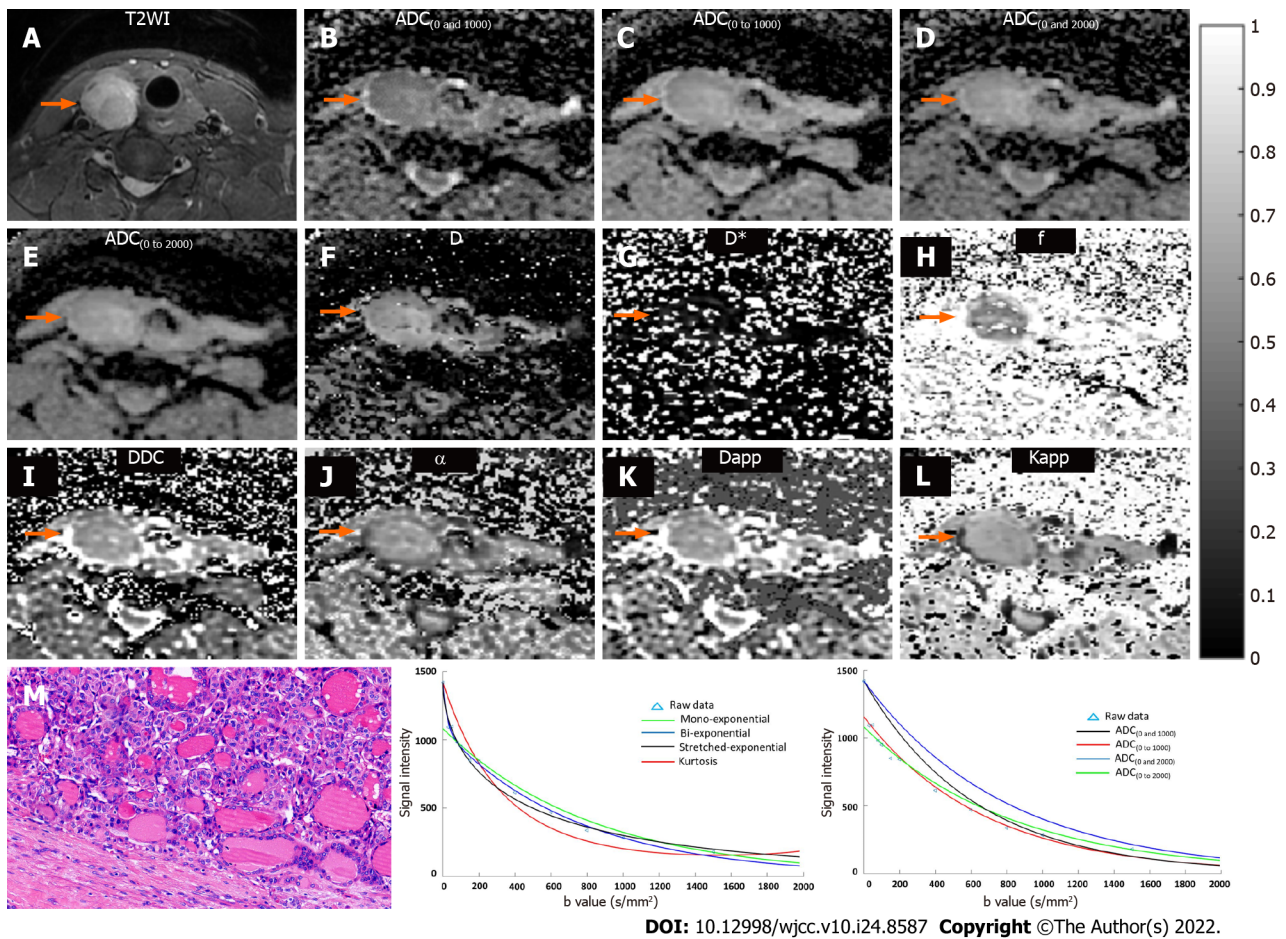


Figure 1 Data from a 49-year-old female with a benign nodule of thyroid adenoma in the right lateral of thyroid. A: T2WI shows the lesion in the right lateral of thyroid (orange arrow). Multiparametric diffusion parameter maps fitted by mono-exponential [B = $ADC_{(0 \text{ and } 1000)}$; C = $ADC_{(0 \text{ to } 1000)}$; D = $ADC_{(0 \text{ and } 2000)}$; E = $ADC_{(0 \text{ to } 2000)}$], bi-exponential (F = D; G = D^* ; H = f), stretched exponential (I = DDC; J = α), and kurtosis diffusion-weighted imaging (K = Dapp; L = Kapp) models show the lesion in the right lateral of thyroid (orange arrow); M: Histopathological H&E image (original magnification, 200 \times) demonstrate abundant colloid and benign-appearing follicular cells; N: Plot of the decay of diffusion weighted signal intensity fitted by a mono-exponential (green), biexponential (blue), stretched-exponential (dark), and kurtosis (red) models for the nodule; O: Plot of the decay of diffusion weighted signal intensity fitted by a mono-exponential with b = 0 and 1000 (dark), b = 0 to 1000 (red), b = 0 and 2000 (blue), and b = 0 to 2000 (green) for the nodule. ADC: Apparent diffusion coefficient; D: Slow diffusion coefficient; D^* : Fast diffusion coefficient; f: Fraction of fast diffusion; DDC: Distributed diffusion coefficient; α : Anomalous exponent term; Dapp: Mean diffusivity; Kapp: Mean kurtosis; ROC: Receiver operating characteristic.

Recently, the potential utility of DKI using higher b values rather than conventional DWI has been reported for detecting pathological alterations in tissue diffusion properties in neural diseases and oncologic applications[33]. Our study showed that malignant thyroid lesions had significantly lower Dapp and higher Kapp values than benign lesions, similar to the results reported by Shi *et al*[34]. This finding might be because the malignant group had lesions with higher cell density than those in the benign group, which contributed to restriction of water diffusion in the extracellular space. Moreover, Shi *et al*[34] found that quantitative DKI was superior to conventional DWI because the Dapp value corrected by the DKI model showed a greater AUC than the ADC, and Kapp showed a higher sensitivity than the ADC. However, in our study, Kapp achieved the highest AUC of 0.889 with a higher sensitivity of 100% than ADC, but the diagnostic performance of those two parameters was not significantly different. Kapp may be a promising indicator with good diagnostic performance.

This study has several limitations. First, the study sample included was relatively small, especially the sample of patients with thyroid cancer, which is a possible reason that may account for the 100% sensitivity or specificity in the ROC curve analysis results. Our findings need to be validated in a larger and more heterogeneous cohort that includes a wider spectrum of thyroid tumor types. Second, regarding the patients in our study, the benign group included only patients with solid nodular goiter and thyroid adenoma, rather than those with all types of benign nodules. In addition, the malignant group did not include all types of thyroid cancer; thus, this may have resulted in some selection bias because of histopathological heterogeneity of thyroid nodules. Third, we selected only the solid regions of the lesion instead of the entire lesion, which may have resulted in some selection bias because of histopathological heterogeneity.

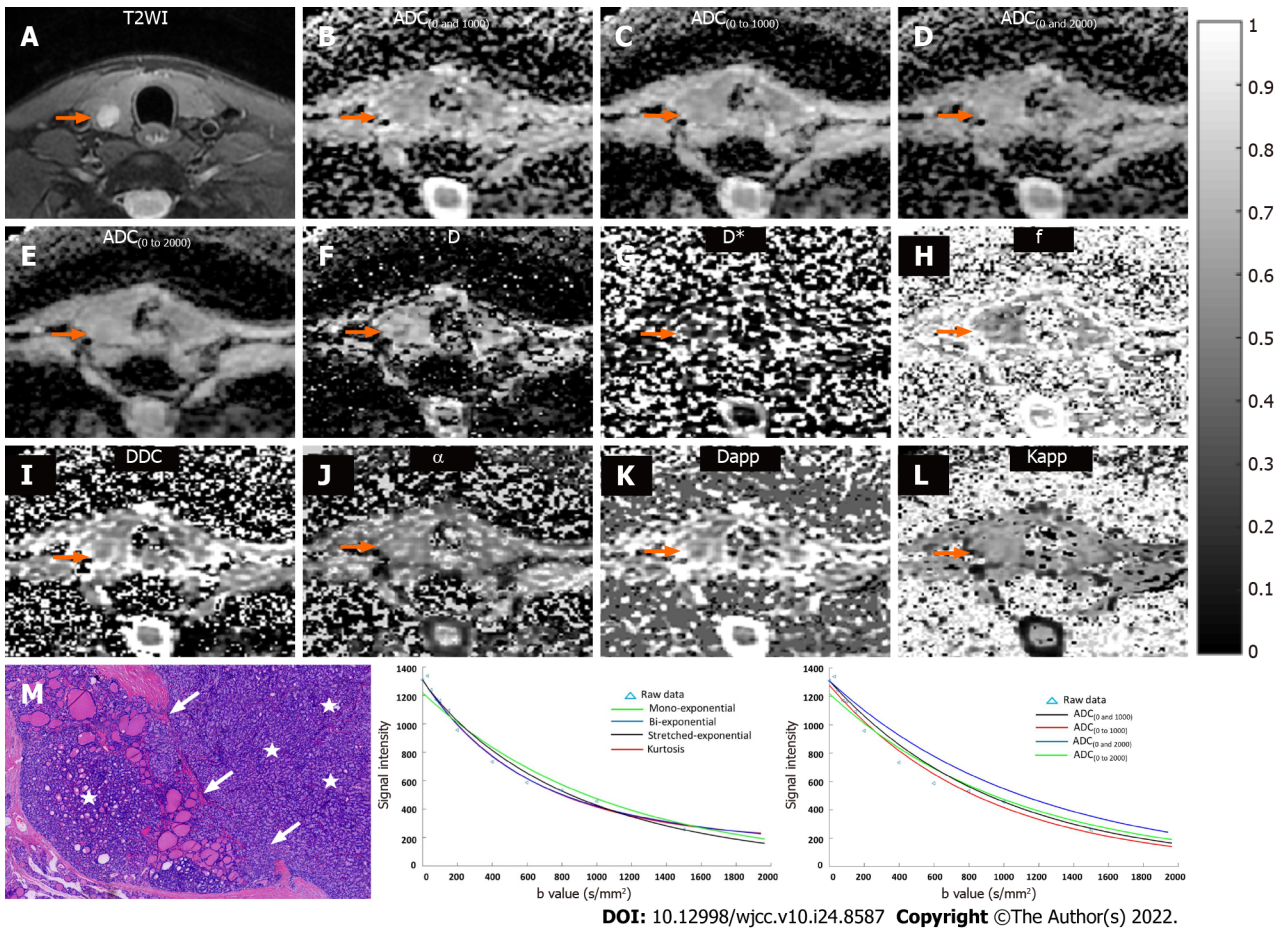


Figure 2 Data from a 35-year-old male with a malignant nodule of follicular thyroid carcinoma in the right lateral of thyroid. A: T2WI shows the lesion in the right lateral of thyroid (orange arrow). Multiparametric diffusion parameter maps fitted by mono-exponential [B = ADC_(0 and 1000); C = ADC_(0 to 1000); D = ADC_(0 and 2000); E = ADC_(0 to 2000)], bi-exponential (F = D; G = D*; H = f), stretched exponential (I = DDC; J = α), and kurtosis diffusion-weighted imaging (K = Dapp; L = Kapp) models show the lesion in the right lateral of thyroid (orange arrow); M: Histopathological H&E image (original magnification, 40×) demonstrate high cell density (stars) and capsular invasion (white arrow); N: Plot of the decay of diffusion weighted signal intensity fitted by a mono-exponential (green), biexponential (blue), stretched-exponential (dark), and kurtosis (red) models for the nodule; O: Plot of the decay of diffusion weighted signal intensity fitted by a mono-exponential with b = 0 and 1000 (dark), b = 0 to 1000 (red), b = 0 and 2000 (blue), and b = 0 to 2000 (green) for the nodule. ADC: Apparent diffusion coefficient; D: Slow diffusion coefficient; D*: Fast diffusion coefficient; f: Fraction of fast diffusion; DDC: Distributed diffusion coefficient; α: Anomalous exponent term; Dapp: Mean diffusivity; Kapp: Mean kurtosis; ROC: Receiver operating characteristic.

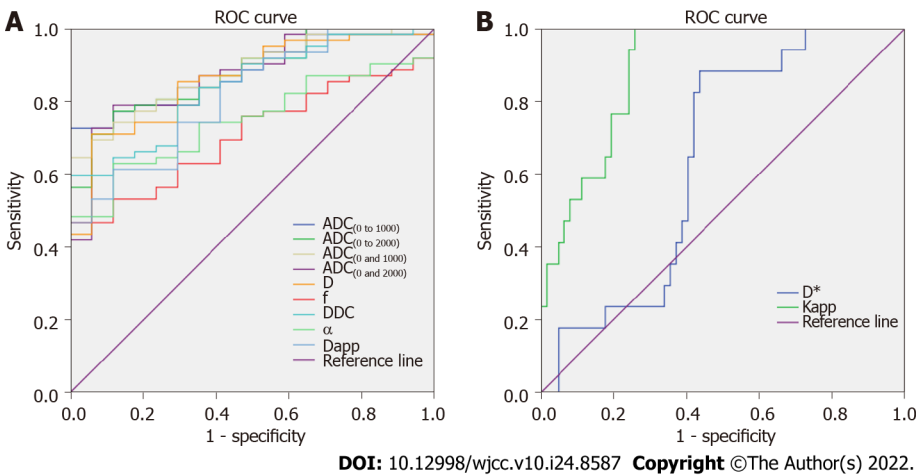


Figure 3 Receiver operating characteristic curve analysis of different diffusion parameters for differentiating malignant thyroid nodules from benign thyroid nodules. ADC: Apparent diffusion coefficient; D: Slow diffusion coefficient; D*: Fast diffusion coefficient; f: Fraction of fast diffusion; DDC: Distributed diffusion coefficient; α: Anomalous exponent term; Dapp: Mean diffusivity; Kapp: Mean kurtosis; ROC: Receiver operating characteristic.

CONCLUSION

In conclusion, our study demonstrates the following: (1) Multiple diffusion coefficient parameters obtained by fitting with mono-exponential, biexponential, stretched exponential, and kurtosis DWI models are feasible techniques for investigating thyroid nodules; (2) The metrics including D, DDC, Dapp and Kapp provide additional information with similar diagnostic performance of ADC, and combination of these metrics may contribute to differentiate benign and malignant thyroid nodules; and (3) the ADC calculated with a mono-exponential model using a single pair of conventional b values ($b = 1000 \text{ s/mm}^2$) have similar diagnostic performance to those calculated with higher b values ($b \text{ value} > 1000 \text{ s/mm}^2$). Clinically, therefore, for the institution has ability to generate higher b values for DWI, the metrics of D, DDC, Dapp and Kapp could be evaluated, which might provide additional information; otherwise, using a single pair of conventional b values ($b = 1000 \text{ s/mm}^2$) still remained a valuable diffusion parameter for differentiating malignant thyroid nodules from benign thyroid nodules.

ARTICLE HIGHLIGHTS

Research background

The value of multiparameter diffusion-weighted imaging (DWI) in quantitative evaluation of thyroid nodule has not been clarified.

Research motivation

It provides a new idea for differentiating benign and malignant thyroid results by using multiparametric diffusion-weighted imaging.

Research objectives

To provide a non-invasive diagnostic means for differentiating benign and malignant thyroid nodules by multiparametric DWI, furthermore, we elucidated which parameters have diagnostic function in differentiating the nature of thyroid nodule

Research methods

We obtained Multiple DWI parameters by patients who underwent multi-b value diffusion-weighted imaging of the thyroid, then the data of benign and malignant nodules were obtained and analyzed.

Research results

Malignant lesions displayed lower diffusion parameters including apparent diffusion coefficient (ADC), the true diffusion coefficient (D), the perfusion fraction (f), the distributed diffusion coefficient (DDC), the intravoxel water diffusion heterogeneity (α) and kurtosis model-derived ADC (Dapp), and higher apparent diffusional kurtosis (Kapp) than benign entities (all $P < 0.01$). The area under the ROC curve (AUC) of the $ADC_{(0 \text{ and } 1000)}$ was significantly higher than the AUC of D^* , f and α (all $P < 0.05$) for differentiating benign from malignant lesions.

Research conclusions

The metrics including D, DDC, Dapp and Kapp provide additional information with similar diagnostic performance of ADC, combination of these metrics may contribute to differentiate benign and malignant thyroid nodules.

Research perspectives

In the future, multiple parameters of magnetic resonance diffusion can be used to accurately distinguish benign and malignant thyroid nodules.

FOOTNOTES

Author contributions: Zhu X and Han J designed the research study; Wang J and Wang YC performed the research; Zhu ZF and Tang J contributed software and formal analysis; Wen XW and Fang Y analyzed the data; Zhu X and Han J wrote the manuscript; all authors have read and approve the final manuscript.

Supported by the Health Commission of Zhejiang Province, No. 2019KY690.

Institutional review board statement: The study was reviewed and approved by the First Hospital of Jiaxing Research and Ethics Committee [(Approval No.2017-226)].

Clinical trial registration statement: The clinical trial is registered with Chinese Clinical Trial Registry, using identifier

ChiCTR2200061944. Details can be found at <http://www.chictr.org.cn/index.aspx>.

Informed consent statement: All study participants, or their legal guardian, provided written consent prior to study enrollment.

Conflict-of-interest statement: All the authors declare no conflict of interest.

Data sharing statement: No additional data are available.

CONSORT 2010 statement: The authors have read the CONSORT Statement – checklist of items, and the manuscript was prepared and revised according to the CONSORT Statement – checklist of items.

Open-Access: This article is an open-access article that was selected by an in-house editor and fully peer-reviewed by external reviewers. It is distributed in accordance with the Creative Commons Attribution NonCommercial (CC BY-NC 4.0) license, which permits others to distribute, remix, adapt, build upon this work non-commercially, and license their derivative works on different terms, provided the original work is properly cited and the use is non-commercial. See: <https://creativecommons.org/licenses/by-nc/4.0/>

Country/Territory of origin: China

ORCID number: Xiang Zhu 0000-0001-7109-8349; Jia Wang 0000-0002-3741-3816; Yan-Chun Wang 0000-0002-4756-3367; Ze-Feng Zhu 0000-0002-1328-1230; Jian Tang 0000-0002-5180-0927; Xiao-Wei Wen 0000-0001-8068-0074; Ying Fang 0000-0002-9277-2037; Jun Han 0000-0002-4821-0547.

S-Editor: Liu JH

L-Editor: A

P-Editor: Liu JH

REFERENCES

- 1 **Fisher SB**, Perrier ND. The incidental thyroid nodule. *CA Cancer J Clin* 2018; **68**: 97-105 [PMID: 29369334 DOI: 10.3322/caac.21447]
- 2 **Paschke R**, Hegedüs L, Alexander E, Valcavi R, Papini E, Gharib H. Thyroid nodule guidelines: agreement, disagreement and need for future research. *Nat Rev Endocrinol* 2011; **7**: 354-361 [PMID: 21364517 DOI: 10.1038/nrendo.2011.1]
- 3 **Schob S**, Meyer HJ, Dieckow J, Pervinder B, Pazaitis N, Höhn AK, Garnov N, Horvath-Rizea D, Hoffmann KT, Surov A. Histogram Analysis of Diffusion Weighted Imaging at 3T is Useful for Prediction of Lymphatic Metastatic Spread, Proliferative Activity, and Cellularity in Thyroid Cancer. *Int J Mol Sci* 2017; **18** [PMID: 28417929 DOI: 10.3390/ijms18040821]
- 4 **Wiltshire JJ**, Drake TM, Uttley L, Balasubramanian SP. Systematic Review of Trends in the Incidence Rates of Thyroid Cancer. *Thyroid* 2016; **26**: 1541-1552 [PMID: 27571228 DOI: 10.1089/thy.2016.0100]
- 5 **Lubitz CC**, Sosa JA. The changing landscape of papillary thyroid cancer: Epidemiology, management, and the implications for patients. *Cancer* 2016; **122**: 3754-3759 [PMID: 27517675 DOI: 10.1002/ncr.30201]
- 6 **Udelsman R**, Zhang Y. The epidemic of thyroid cancer in the United States: the role of endocrinologists and ultrasounds. *Thyroid* 2014; **24**: 472-479 [PMID: 23937391 DOI: 10.1089/thy.2013.0257]
- 7 **Haugen BR**. 2015 American Thyroid Association Management Guidelines for Adult Patients with Thyroid Nodules and Differentiated Thyroid Cancer: What is new and what has changed? *Cancer* 2017; **123**: 372-381 [PMID: 27741354 DOI: 10.1002/ncr.30360]
- 8 American Thyroid Association (ATA) Guidelines Taskforce on Thyroid Nodules and Differentiated Thyroid Cancer, Cooper DS, Doherty GM, Haugen BR, Kloos RT, Lee SL, Mandel SJ, Mazzaferri EL, McIver B, Pacini F, Schlumberger M, Sherman SI, Steward DL, Tuttle RM. Revised American Thyroid Association management guidelines for patients with thyroid nodules and differentiated thyroid cancer. *Thyroid* 2009; **19**: 1167-1214 [PMID: 19860577 DOI: 10.1089/thy.2009.0110]
- 9 **Hao Y**, Pan C, Chen W, Li T, Zhu W, Qi J. Differentiation between malignant and benign thyroid nodules and stratification of papillary thyroid cancer with aggressive histological features: Whole-lesion diffusion-weighted imaging histogram analysis. *J Magn Reson Imaging* 2016; **44**: 1546-1555 [PMID: 27093648 DOI: 10.1002/jmri.25290]
- 10 **Tan H**, Chen J, Zhao YL, Liu JH, Zhang L, Liu CS, Huang D. Feasibility of Intravoxel Incoherent Motion for Differentiating Benign and Malignant Thyroid Nodules. *Acad Radiol* 2019; **26**: 147-153 [PMID: 29908978 DOI: 10.1016/j.acra.2018.05.011]
- 11 **Suo S**, Cheng F, Cao M, Kang J, Wang M, Hua J, Hua X, Li L, Lu Q, Liu J, Xu J. Multiparametric diffusion-weighted imaging in breast lesions: Association with pathologic diagnosis and prognostic factors. *J Magn Reson Imaging* 2017; **46**: 740-750 [PMID: 28139036 DOI: 10.1002/jmri.25612]
- 12 **Bennett KM**, Schmainda KM, Bennett RT, Rowe DB, Lu H, Hyde JS. Characterization of continuously distributed cortical water diffusion rates with a stretched-exponential model. *Magn Reson Med* 2003; **50**: 727-34. [PMID: 14523958 DOI: 10.1002/mrm.10581]
- 13 **Ertas G**, Onaygil C, Akin Y, Kaya H, Aribal E. Quantitative differentiation of breast lesions at 3T diffusion-weighted imaging (DWI) using the ratio of distributed diffusion coefficient (DDC). *J Magn Reson Imaging* 2016; **44**: 1633-1641

- [PMID: 27284961 DOI: 10.1002/jmri.25327]
- 14 **Wang F**, Wang Y, Zhou Y, Liu C, Xie L, Zhou Z, Liang D, Shen Y, Yao Z, Liu J. Comparison between types I and II epithelial ovarian cancer using histogram analysis of monoexponential, biexponential, and stretched-exponential diffusion models. *J Magn Reson Imaging* 2017; **46**: 1797-1809 [PMID: 28379611 DOI: 10.1002/jmri.25722]
 - 15 **Senn S**. Review of Fleiss, statistical methods for rates and proportions. *Res Synth Methods* 2011; **2**: 221-222 [PMID: 26061787 DOI: 10.1002/jrsm.50]
 - 16 **Wu Y**, Yue X, Shen W, Du Y, Yuan Y, Tao X, Tang CY. Diagnostic value of diffusion-weighted MR imaging in thyroid disease: application in differentiating benign from malignant disease. *BMC Med Imaging* 2013; **13**: 23 [PMID: 23899414 DOI: 10.1186/1471-2342-13-23]
 - 17 **Dilli A**, Ayaz UY, Cakir E, Cakal E, Gultekin SS, Hekimoglu B. The efficacy of apparent diffusion coefficient value calculation in differentiation between malignant and benign thyroid nodules. *Clin Imaging* 2012; **36**: 316-322 [PMID: 22726970 DOI: 10.1016/j.clinimag.2011.10.006]
 - 18 **Shi HF**, Feng Q, Qiang JW, Li RK, Wang L, Yu JP. Utility of diffusion-weighted imaging in differentiating malignant from benign thyroid nodules with magnetic resonance imaging and pathologic correlation. *J Comput Assist Tomogr* 2013; **37**: 505-510 [PMID: 23863524 DOI: 10.1097/RCT.0b013e31828d28f0]
 - 19 **Lu Y**, Hatzoglou V, Banerjee S, Stambuk HE, Gonen M, Shankaranarayanan A, Mazaheri Y, Deasy JO, Shaha AR, Tuttle RM, Shukla-Dave A. Repeatability Investigation of Reduced Field-of-View Diffusion-Weighted Magnetic Resonance Imaging on Thyroid Glands. *J Comput Assist Tomogr* 2015; **39**: 334-339 [PMID: 25700226 DOI: 10.1097/RCT.0000000000000227]
 - 20 **Purroy F**, Begue R, Quilez A, Sanahuja J, Gil MI. Contribution of high-b-value diffusion-weighted imaging in determination of brain ischemia in transient ischemic attack patients. *J Neuroimaging* 2013; **23**: 33-38 [PMID: 22309574 DOI: 10.1111/j.1552-6569.2011.00696.x]
 - 21 **Doskaliyev A**, Yamasaki F, Ohtaki M, Kajiwara Y, Takeshima Y, Watanabe Y, Takayasu T, Amatya VJ, Akiyama Y, Sugiyama K, Kurisu K. Lymphomas and glioblastomas: differences in the apparent diffusion coefficient evaluated with high b-value diffusion-weighted magnetic resonance imaging at 3T. *Eur J Radiol* 2012; **81**: 339-344 [PMID: 21129872 DOI: 10.1016/j.ejrad.2010.11.005]
 - 22 **Ning P**, Shi D, Sonn GA, Vasanaawala SS, Loening AM, Ghanouni P, Obara P, Shin LK, Fan RE, Hargreaves BA, Daniel BL. The impact of computed high b-value images on the diagnostic accuracy of DWI for prostate cancer: A receiver operating characteristics analysis. *Sci Rep* 2018; **8**: 3409 [PMID: 29467370 DOI: 10.1038/s41598-018-21523-6]
 - 23 **Eghtedari M**, Ma J, Fox P, Guvenc I, Yang WT, Dogan BE. Effects of magnetic field strength and b value on the sensitivity and specificity of quantitative breast diffusion-weighted MRI. *Quant Imaging Med Surg* 2016; **6**: 374-380 [PMID: 27709073 DOI: 10.21037/qims.2016.07.06]
 - 24 **Le Bihan D**, Turner R. The capillary network: a link between IVIM and classical perfusion. *Magn Reson Med* 1992; **27**: 171-178 [PMID: 1435202 DOI: 10.1002/mrm.1910270116]
 - 25 **Zhang SX**, Jia QJ, Zhang ZP, Liang CH, Chen WB, Qiu QH, Li H. Intravoxel incoherent motion MRI: emerging applications for nasopharyngeal carcinoma at the primary site. *Eur Radiol* 2014; **24**: 1998-2004 [PMID: 24838795 DOI: 10.1007/s00330-014-3203-0]
 - 26 **Pesapane F**, Patella F, Fumarola EM, Panella S, Ierardi AM, Pompili GG, Franceschelli G, Angileri SA, Magenta Biasina A, Carrafiello G. Intravoxel Incoherent Motion (IVIM) Diffusion Weighted Imaging (DWI) in the Periferic Prostate Cancer Detection and Stratification. *Med Oncol* 2017; **34**: 35 [PMID: 28144814 DOI: 10.1007/s12032-017-0892-7]
 - 27 **Liang L**, Luo X, Lian Z, Chen W, Zhang B, Dong Y, Liang C, Zhang S. Lymph node metastasis in head and neck squamous carcinoma: Efficacy of intravoxel incoherent motion magnetic resonance imaging for the differential diagnosis. *Eur J Radiol* 2017; **90**: 159-165 [PMID: 28583628 DOI: 10.1016/j.ejrad.2017.02.039]
 - 28 **Tezelman S**, Giles Y, Tunca F, Gok K, Poyanli A, Salmaslioglu A, Terzioglu T. Diagnostic value of dynamic contrast medium enhanced magnetic resonance imaging in preoperative detection of thyroid carcinoma. *Arch Surg* 2007; **142**: 1036-1041 [PMID: 18025330 DOI: 10.1001/archsurg.142.11.1036]
 - 29 **Patel J**, Sigmund EE, Rusinek H, Oei M, Babb JS, Taouli B. Diagnosis of cirrhosis with intravoxel incoherent motion diffusion MRI and dynamic contrast-enhanced MRI alone and in combination: preliminary experience. *J Magn Reson Imaging* 2010; **31**: 589-600 [PMID: 20187201 DOI: 10.1002/jmri.22081]
 - 30 **Lemke A**, Laun FB, Simon D, Stieltjes B, Schad LR. An *in vivo* verification of the intravoxel incoherent motion effect in diffusion-weighted imaging of the abdomen. *Magn Reson Med* 2010; **64**: 1580-1585 [PMID: 20665824 DOI: 10.1002/mrm.22565]
 - 31 **Liu X**, Zhou L, Peng W, Wang H, Zhang Y. Comparison of stretched-Exponential and monoexponential model diffusion-weighted imaging in prostate cancer and normal tissues. *J Magn Reson Imaging* 2015; **42**: 1078-1085 [PMID: 25727776 DOI: 10.1002/jmri.24872]
 - 32 **Liu C**, Wang K, Li X, Zhang J, Ding J, Spuhler K, Duong T, Liang C, Huang C. Breast lesion characterization using whole-lesion histogram analysis with stretched-exponential diffusion model. *J Magn Reson Imaging* 2018; **47**: 1701-1710 [PMID: 29165847 DOI: 10.1002/jmri.25904]
 - 33 **Minosse S**, Marzi S, Piludu F, Vidiri A. Correlation study between DKI and conventional DWI in brain and head and neck tumors. *Magn Reson Imaging* 2017; **42**: 114-122 [PMID: 28629955 DOI: 10.1016/j.mri.2017.06.006]
 - 34 **Shi RY**, Yao QY, Zhou QY, Lu Q, Suo ST, Chen J, Zheng WJ, Dai YM, Wu LM, Xu JR. Preliminary study of diffusion kurtosis imaging in thyroid nodules and its histopathologic correlation. *Eur Radiol* 2017; **27**: 4710-4720 [PMID: 28616727 DOI: 10.1007/s00330-017-4874-0]



Published by **Baishideng Publishing Group Inc**
7041 Koll Center Parkway, Suite 160, Pleasanton, CA 94566, USA
Telephone: +1-925-3991568
E-mail: bpgoffice@wjgnet.com
Help Desk: <https://www.f6publishing.com/helpdesk>
<https://www.wjgnet.com>

